ISSN: 0067-2904

Green Synthesis of Copper Nanoparticles Using Tea Leaves Extract to Remove Ciprofloxacin (CIP) from Aqueous Media

Mohammed A. Atiya[1], Ahmed K. Hassan*[2], Fatimah Q. Kadhim[1]
[1]Al-Khwarizmi College of Engineering, University of Baghdad, Baghdad, Iraq
[2]Environment and Water Directorate, Ministry of Science and Technology, Baghdad, Iraq

Received: 4/10/2020 Accepted: 7/2/2021

Abstract

In the present investigation, the synthesis of copper nanoparticles from green tea was attempted and investigated for its capacity to adsorb drugs (Ciprofloxacin). The copper nanoparticles (Cu-NPs) were characterized by different techniques of analysis such as scanning electron microscopy (SEM) images, atomic force microscope (AFM), blumenauer-emmer-teller **(**BET), fourier transform infrared (FTIR) spectroscopy, and zeta potentials techniques. Cu-NPs lie in the mesoporous material category with a diameter in the range of 2-50 nm. The aqueous solution was investigated for the removal of ciprofloxacin (CIP) with green tea-synthesized Cu-NPs. The results showed that ciprofloxacin efficiency depends on initial pH (2.5-10), CIP (2mg/L-15mg / L) dose, temperature (20 ° C-50 ° C); time (0-180 min) and Cu-NP dose (0.1g /L-1g /L). Spherical nanoparticles with an average size of 47nm and a surface area of 1.6562m^2/g were synthesized. The batch experiment showed that 92% of CIP 0.01 mg/L were removed at a maximum adsorbent dose of 0.75 g/L, pH 4, 180 min, and an initial 1:1 rate (w / w) of CIP: Cu-NPs. Kinetic adsorption models and ciprofloxacin removal mechanisms were examined. The kinetic analysis showed that adsorption is a physical adsorption system with activation energy of 0.8409 kJ.mol^{-1}. A pseudo-first-order model is preferred for the kinetic removal after the physically diffusing process due to the low activation energy of 13.221kJ.mol^{-1}. On the other hand, Langmuir, Freundlich, Temkin, and Dubinin isotherm models were also studied; the equilibrium data were best fitted with Langmuir and Dubinin isotherm models with maximum adsorption capacity of 5.5279, and 1.1069 mg/g, respectively. The thermodynamic values of ΔG^0 were -0.0166, -0.0691, -4.1084, and -0.7014 kJ/mol at 20, 30, 40, and 50 ° C, respectively. The values of ΔH^0 and ΔS^0 were 18.8603 kJ/mol and 0.0652kJ/mol.k, respectively. These values showed spontaneous and endothermic sorption. The presence of the CIP concentration in aqueous media was identified by UV-analysis.

Keywords: Green tea, Ciprofloxacin, Adsorption, Kinetics, Isotherm, Thermodynamics

التخليق الاخضر لدقائق النحاس النانوية باستخدام مستخلص اوراق الشاي لازالة مادة السبروفلاكساسين من المحلول المائي

محمد عبد عطية[1]، احمد خضيرقاسم كاظم[2*]، فاطمه قاسم كاظم[1]
[1]كلية الهندسة الخوارزمي، جامعة بغداد، بغداد، العراق
[2]دائرة البيئة والمياه، وزارة العلوم والتكنلوجيا، بغداد، العراق

*Email: qaf2622@gmail.com

الخلاصة

تهدف الدراسة الحالية الى تخليق جزيئات النحاس النانوية من الشاي الاخضر واستخدامه كمادة مازة لإزالة المادة الدوائية سيبروفلوكساسين . تم فحص جزيئات النحاس بواسطة تقنيات مختلفة مثل SEM, AFM, BET, FTIR, Zeta Potential و من خلال فحص التركيب المسامي لجزيئات النحاس النانوية تبين انه ذو تركيب mesoporous أي ذو اقطار مسامية تتراوح بين 2− 50nm . تم التحقيق في المحلول المائي لإزالة سيبروفلوكساسين (CIP) مع النحاس النانوي للشاي الاخضر. اظهرت النتائج ان كفاءة سيبروفلوكساسين تعتمد على درجة الحموضة (2.5−10), جرعة المادة الدوائية (سيبروفلوكساسين) (2−15مغم/لتر), درجة الحرارة (20− 50 درجة مئوية), الوقت (0−180 دقيقة) وجرعة النحاس النانوي (0.1−1 غم/لتر). تكون الجسيمات النانوية كروية الشكل وبمتوسط حجم 47 نانومتر ومساحة سطحية تبلغ 1.6562 متر^2/غم. اظهرت التجارب ان ازالة 0.01 مغم/لتر تبلغ 92% و وزن المادة المازة 0.75غم/لتر عند اقصى درجة حموضة 4 خلال 180 دقيقة بمعدل اولي 1:1 كنسبة وزنية ل(وزن المادة الدوائية/ وزن جزيئات النحاس النانوية) . تم فحص نماذج الامتزاز الحركية الزائفة واليات ازالة السيبروفلوكساسين. اظهر التحليل الحركي ان الامتزاز هو نظام فيزيائي بطاقة تنشيط تبلغ 0.8409 كيلوجول/مول. المعادلة النموذجية الزائفة من الدرجة الاولى تكون مفضلة بطاقة تنشيط واطئة 13.22كيلو جول/مول ويكون الانتشار فيزيائي. من ناحية اخرى تم دراسة موديلات لانكماير, فريندلخ, تيمكنو دوبينن ووجد انها توافق موديل لانكماير و دوبينن وان قيمة قابلية الامتزاز القصوى هي 5.5279 و 1.1069. تم حساب ديناميكية الحرارية واظهرت النتائج قيمة طاقة كبس الحرة (0.0166− , 0.7014− and 4.1084−, 0.0691 كيلو جول/مول) عند درجات الحرارة 20, 30, 40 و50 درجة مئوية). قيمة الانثالبي والانتروبي 18.8603و 0.0652 كيلو جول/ مول.كلفن). اظهرت النتائج ان الامتزاز يكون ماص للحرارة وتلقائي. التحقق من وجود تركيز المادة الدوائية سيبروفلوكساسين يتم بواسطة جهاز UV.

1. Introduction

Increasing the risk of health because of indiscriminate drug disposal in aqueous environments and drug contamination of the groundwater system has been a major cause for concern because of harmful environmental effects [1]. Many pharmaceutical industries release toxic contaminants directly or after chemical modifications into the environment [2]. Fluoroquinolones have been usually detected in an aqueous environment within the range of 1-100 mg /L [3]. Ciprofloxacin {(1-Cyclopropyl-6-fluoro-4-oxo-7-(piperazine-1-yl)-1, 4-dihydroquinoline-3-carboxylic acid hydrochloride hydrate)} is a commonly used broad-spectrum antibiotic agent of the fluoroquinolone family [3]. Also, the waste from hospitals, housekeepers, and human excretion contributes to drug contamination [1]. The potential presence of antibiotics in water sources is of major concern because of the unknown health consequences from chronically low levels of antibiotics exposure throughout the life of the drinking water, if the antibiotics survive and remain in the drinking water of consumers [3]. These antibiotics have been detected in wastewater in very low levels, but also highly toxic to human, animal, and aquatic life , causing health problems like headache, diarrhea, tremors, nausea, vomiting, etc. Several methods for fluoroquinolone removal have been identified, including photo-catalysis [4], advanced oxidation [5], and adsorption using various adsorbents, for example, carbon activated [6], sawdust [3], agricultural waste, and titanium oxide [7]. However, adsorption has some advantages among these methods because of its high selectivity, high removal efficiency, easy operation, and lower costs [5]. This process uses the so-called "sorbent, adsorbent, or bio-sorbent material," which reduces contaminated solutions in the form of pollutant molecules (so-called adsorbates) [8, 9]. To include the adsorbent process in terms of removal efficiency and cost-effectiveness [10, 11], care should be taken to choose adsorbents. Nanotechnology can be defined as the physical and biological processes performed for the handling of material to create materials with special properties for use in various applications [12]. Usually, nanotechnology deals with handling low-size materials below 100 nm.

Nanomaterials are small products with a broad area of volume that are primarily responsible for the widespread use of nanomaterials in the electronic, mechanical, optical, microbiological, biotechnological, healthcare, environmental, engineering, and many other sectors [13]. Green synthesis is a simple alternative to chemical synthesis, using either bio-organisms or plant extracts. Green synthesis offers advances compared to chemical processes because it makes it easy to extend to

large-scale systems with an environmental, economic, and efficient environment. In green synthesis, typically three major steps are taken: (1) choice of solvent media; (2) choice of eco-friendly reduction agents; and (3) stabilization of nanoparticles with non-toxic substances [14]. Copper nanoparticles were synthesized using plant extract as a reducing agent. Copper nanoparticles have several properties such as low cost, high surface area [15], super-strong structure, antibacterial properties, sensor properties, and catalytic properties [16]. Synthesis of Cu-NPs is cost-effective when compared to that of silver nanoparticle. Due to their surface to volume ratio, copper nanoparticles are highly reactive and easily interact with other particles [17]. The adsorption kinetics was obtained by several models (Pseudo- first order, Pseudo second order, Elovichs [18], and Behnajady-Modirshahla-Ghanbary (BMG)) [19]. The uptake analysis of CIP was studied by applying Langmuir, Freundlich, Temkin, and Dubinin models [18]. The thermodynamic parameters were also studied [20]. The present research is therefore aimed at preparing and distinguishing Cu-NPs. The performance of adsorption of Cu-NPs to the concurrent removal of the antibiotic of ciprofloxacin (CIP) was subsequently studied in detail, taking into consideration the influence of some environmental factors on the adsorption behavior.

2. Materials and Methods

2.1. Chemicals used

Ciprofloxacin used in this study was provided by the Ministry of Industry (Ibn Sina Centre), and Table-1 shows the characteristics of the drug. The maximum wavelength λ (nm) was measured using a spectrophotometer (UV/VIS model 1800 SHIMADZU). The chemical structure of the drug is shown in Figure-1.

Table 1-Main physical and chemical characteristics of Ciprofloxacin (CIP) used in this study [21, 22]

Drug class	**Fluoroquinolone**
IUPAC Name	1-Cyclopropyl-6-fluoro-4-oxo-7-(piperazin-1-yl)-1,4-dihydroquinoline-3-carboxylic acid hydrochloride hydrate
Molecular formula	$C_{17}H_{21}ClFN_3O_4$
Molecular weight (g/mol)	385.82
Color	White
Purity	99.8%
λ_{max} (nm)	276

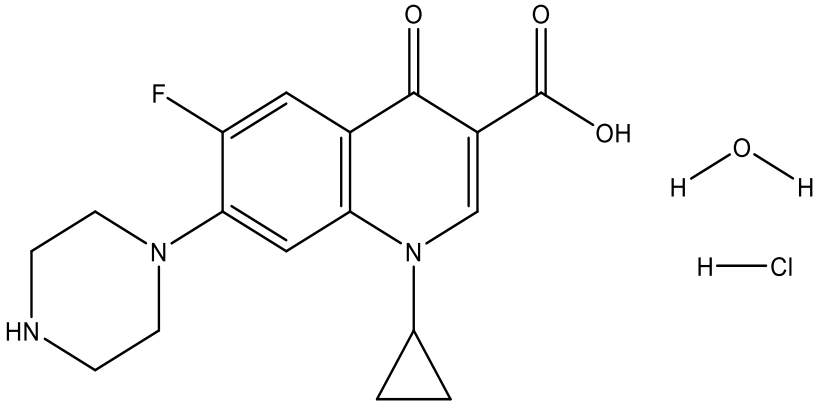

Figure 1-Chemical structure of CIP drug used in this study [21].

2.2. Adsorbent Preparation

The Cu-NPs nanoparticles were prepared using a similar procedure described in previous studies [23, 24, and 25] with some modifications.

The extract of the green tea was prepared by weighing 20.0 g of locally available solid green tea in 300 mL of distilled water. The solution was heated for 30 min at 85°C on a hot plate. The extract was filtered using a 0.45 μm membrane filter to remove the suspended tea particles and stored in the refrigerator at 5°C for further use. A solution of 0.10 M $CuSO_4.5H_2O$ was prepared by adding 4.996 g of solid $CuSO_4.5H_2O$ in 200 mL of distilled water. After complete dissolving, this solution was filtered using a 0.45 μm membrane filter to remove any impurities. The tea extract was mixed with the solution of 0.10 M $CuSO_4.5H_2O$ with a proportion of mixing 4:1 w/w by adding it slowly for 15 min at room temperature and constant stirring. After the addition, the color of the solution was changed from

blow light to green light, and finally, to a dark yellow, while the formation of dark brown precipitation began after 5 min. This color change indicated the reduction of copper nanoparticles. Following this, 0.1 M NaOH solution was added drop by drop until the pH was adjusted at 9.0 and continuously stirred for 15 min [26]. At pH=9, the dark brown copper nanoparticles were highly precipitated in the beaker and could be collected easily. The brawn precipitate of copper particles was collected by vacuum filtration using filter paper (Whatman No.1) and quickly rinsed several times with distilled water and ethanol to remove any unreacted particles. The Cu-NPs nanoparticles were dried overnight in an oven at 60 °C and then were ground to a fine powder.

The green chemical reaction of the reduction of Cu^{2+} to Cu^0 may be similar to the reduction of Fe^{3+} to Fe^0 [24]. The proposed mechanism can be illustrated in the following reaction:

$nCu^{2+} + 2Ar\text{-}(OH)_n \rightarrow nCu^0 + 2nAr_{=}O + 2nH^+$

where Ar is the phenyl group and n is the oxidized hydroxyl group number by Cu^{2+}.

2.3 . Characterization

Scanning electron microscopy (SEM) images of Cu-NPs were performed by using SEM TESCAN-Vega3 model. These images were used to detect changes in surface morphology due to adsorbent synthesis or adsorptions. A Shimadzu FTIR spectroscopy instrument (Japan) identified the functional groups in the Cu-NPs and the importance of them in the removal process. These analyzes were conducted in the region of 400-4000 cm^{-1} of the wavenumber, with the range falling within that of all well-known agriculture adsorption groups. The essential green tea surface area was calculated using the Brunauer – Emmett – Teller (BET) application. The 120 mg Cu-NPs sample was then transmitted onto the BET tube (inner diameter = 0.7 cm) and released in vacuum for 24 hours before BET testing at a temperature of 60 ° C. The zeta potential analysis was used to detect nanoparticle stabilization, which showed that the nanoparticles were more agglomerative with potential negative zeta values. Atomic force microscopy (AFM) was used to measure the dimension and morphology of the surface, which tests the contact force between the tip and the surface.

2.4 Adsorption experiments

A 10 mg / L CIP working solution was prepared by dissolving 0.01 g CIP in 1 L of deionized water. Before adding nanoparticles, the pH of the solution was adjusted. In this study, batch tests were conducted to evaluate the efficiency of CIP removal. The experiments met several working parameters, including pH within the range of 2 to 10, Cu-NPs dosages between 0.1 and 1 g / L, duration of contact of up to 180 min, initial CIP antibiotic concentrations between 2 and 15 mg /L, and temperatures between 20 and 50 °C. A specific amount of Cu-NPs was added to the CIP antibiotic solution, and then it was stirred at 300 rpm in a closed system. The pH of the solution was adjusted by 0.1 M H_2SO_4 and 0.1 M NaOH. Temperature was maintained and the optimized value of each parameter was recorded. 10 mL samples were taken for analysis at different intervals during the adsorption experiments. The initial CIP concentrations were compared with the calibration data obtained immediately upon each sample with UV / VIS spectrophotometer, using a 1cm quartz container with the absorption of 276 nm maximum wavelength. Reference (blank) Cu-NPs solutions were read before each measurement, with the same concentrations as those of the sample. Also, adsorption data on temperature effects in contact times were used with various starting concentrations and sorbent doses, particularly in thermodynamic, kinetic, and isothermal studies. Cu-NPs were evaluated based on the efficiency of removal (R %) and adsorbent capacity ; q_e (mg/g) values for the removal of antibiotic contaminants from water solutions [27, 28].

$$R\ \% = (C_0 - C_t) * 100 / C_0 \quad (1)$$

$$q_e = (C_0 - C_e) * V / W \quad (2)$$

where C_0, C_t, and C_e denote the initial, at a specific time of adsorption, and equilibrium concentrations of CIP aqueous phase antibiotics (mg/L), respectively, V is the antibiotic solution volume in Liter, and W is the Cu-NPs adsorbent in (gm).

The removal mechanism of the CIP onto Cu-NPs depends on the van der Waals forces interaction between adsorbent and adsorbate. As a result, the adsorbate transfers from the liquid phase to the boundary layer of the adsorbent, then the adsorbate transfers from the boundary layer to the external surface of the adsorbent. After that, the adsorbate at the outer surface transfers into the inner surface of the adsorbent by pore diffusion and, finally, the active interaction occurs between the molecules of adsorbate and the adsorbent [3].

In the closed system, several conditions were examined; wide range of the initial pH (2.5, 3, 4, 5, 7, 8, 9, 10), initial CIP concentration (2, 5, 10, 15 mg / L), Cu-NPs dose (0.1, 0.25, 0.75, 1 g / L) and temperature (20, 30, 40, 50 ° C). The performance of CIP removal was determined by Eq. (1).

3. Results and Discussion

3.1. Characterization of Cu-NPs

Scanning electron microscopy was utilized to analyze the structure, composition, and average size of the synthesized copper nanoparticles, as shown in Figure-2. The typical SEM picture demonstrates that the product consists mainly of spherical and monodispersed particles, with size distribution that ranges between 30 nm and 120 nm. Another observation that was noticed with high magnification shows, however, that these Cu-NPs are assembled from smaller and highly uniform nanoparticles with an average diameter of about 21 nm.

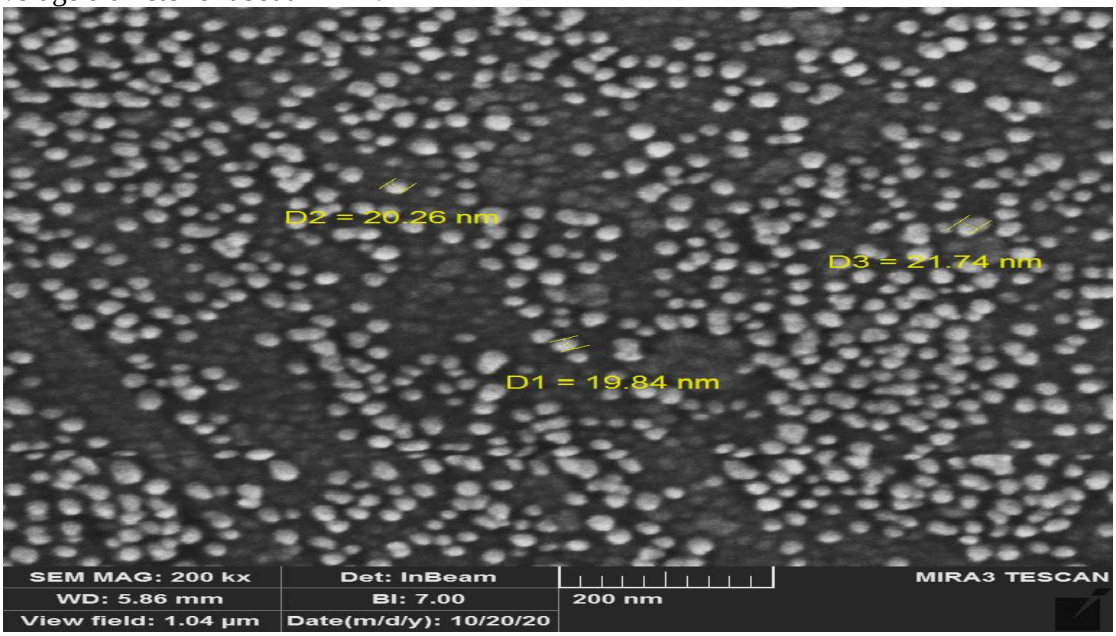

Figure 2-SEM micrograph of Cu-NPs

FTIR spectra of Cu-NPs are shown in Figure-3. For each spectrum, 32 scans at a 4 cm^{-1} resolution were made [20]. Figure-3 shows the wide peak at O-H at 3411 cm^{-1}, which indicates the presence of polyphenols, with the association between C-H asymmetrical stretching and certain signals in 2948, 1782, 1615 and 1029 cm^{-1} assigned for C=O of aromatic rings, C=C stretch, C-O-C and C-OH bending, respectively. Polyphenols can be assumed to work as reduction agents, as well as capping agents, in the green tea extract [29].

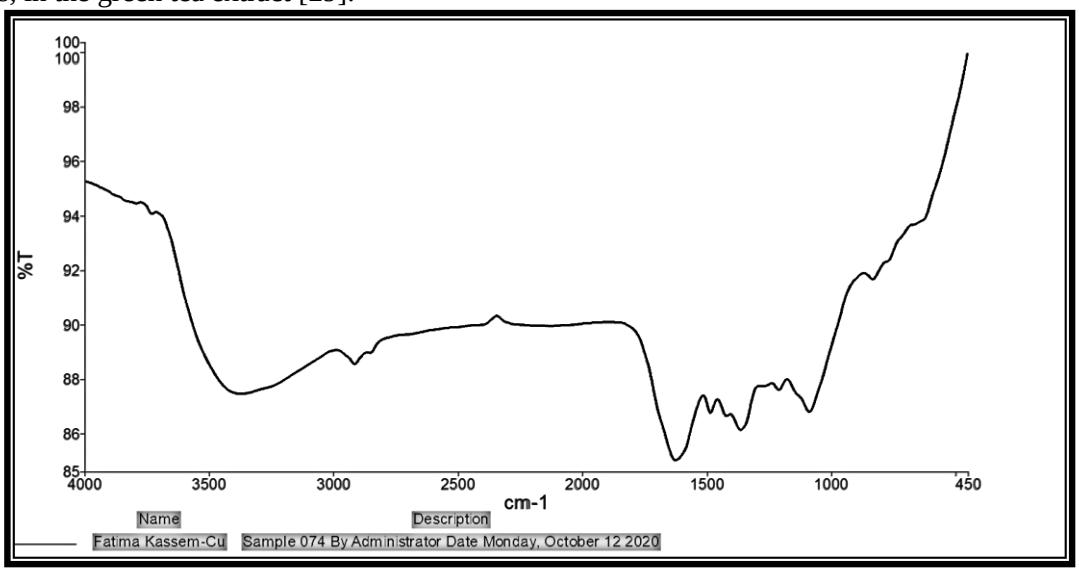

Figure 3-FTIR spectrum of Cu-NPs nanoparticles

Atomic force microscopy (AFM) was used to determine the size and surface morphology of Cu-NPs nanoparticles, testing the contact forces between the tip and surface. The average size of nanoparticles for copper nanoparticles according to the AFM image shown in Figure-4.a is 47 nm. Also, Figure-4.b illustrates Cu-NPs surface morphology as nanoparticles.

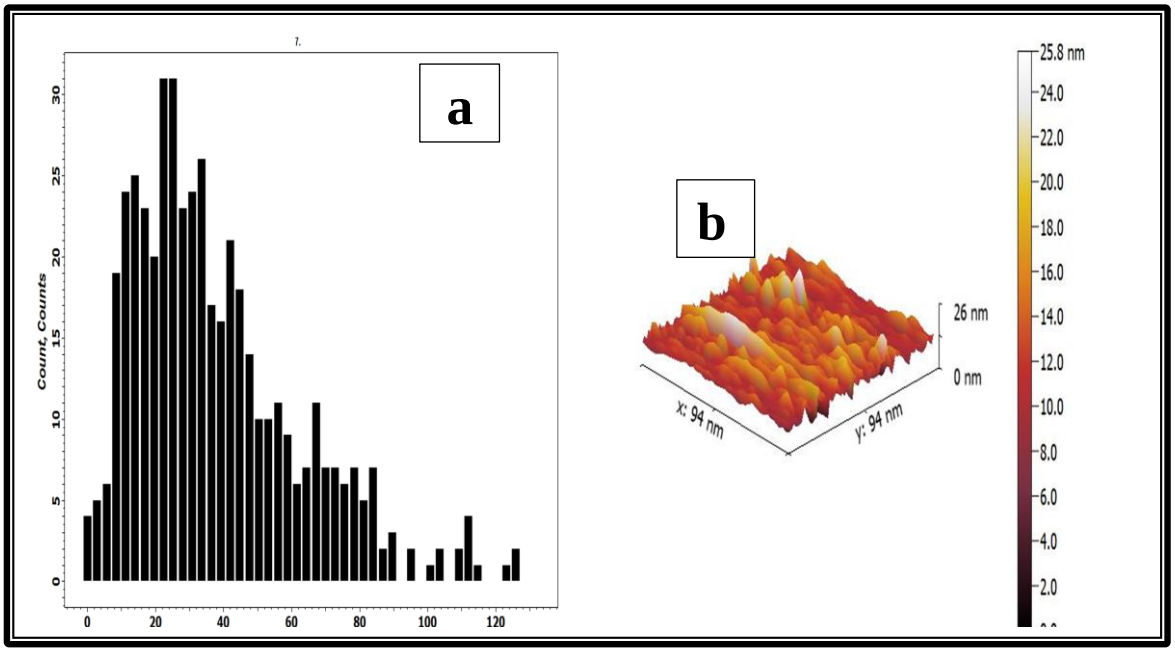

Figure 4- (a) Atomic Force Microscopy of Cu-NPs nanoparticles, **(b)** Cu-NPs surface morphology

As shown in Figure-5, nano fluid stability was characterized by the technique of zeta potential analysis, which shows that the nanoparticles are more agglomerative, with potential negative zeta values of -17.5 mV for Cu-NPs.

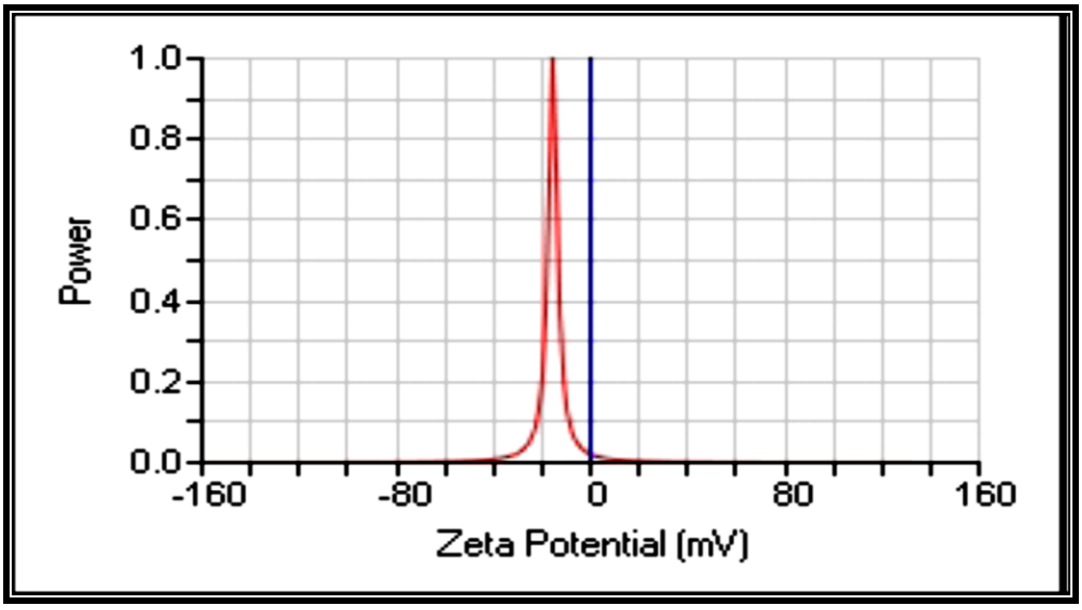

Figure 5- Zeta potential of Cu-NPs nanoparticles

Table-2 describes and clarifies the results of BET test; the pore size for Cu-NPs was 8.2568 nm, which is described as ultramicro. The International Union of Pure and Applied Chemistry (IUPAC) classify the pore size of > 50 nm as macropore, 2-50 nm as mesoporous, and < 0.7nm as supermicropore, also called ultramicropore [30].

Table 2-Results of Blumenauer-Emmer-Teller parameter for Cu-NPs

Parameter	Value
BET (m^2/g)	1.6562
Pore volume(cm^3/g)	0.00839
Pore size (nm)	8.2568

3.2 Removal of CIP at different conditions

3.2.1 Effects of Cu-NPs dose

The adsorbent dose is an important parameter because the capacity of the sorbent for a given initial adsorbent concentration is determined. The effect on ciprofloxacin removal is shown in Figure-6. The percentage of CIP removal raised from 20%, 29%, 41.6%, and 51.4 to 54.1% using different concentrations of Cu-NPs (0.1, 0.25, 0.5, 0.75, and 1 gm, respectively). With higher Cu-NPS concentration, the removal rate and effectiveness for CIP adsorption are increased, with the other parameter being maintained (pH, drug level, time of contact, and temperature).The increase in removal efficiency with the increased Cu-NPs dosage is due to the increase in the total area and the number of active sites [31, 32]. Similar behaviors were also noticed in previous studies [23, 33]. The optimal dose of copper nanoparticles used was 0.75 gm / L.

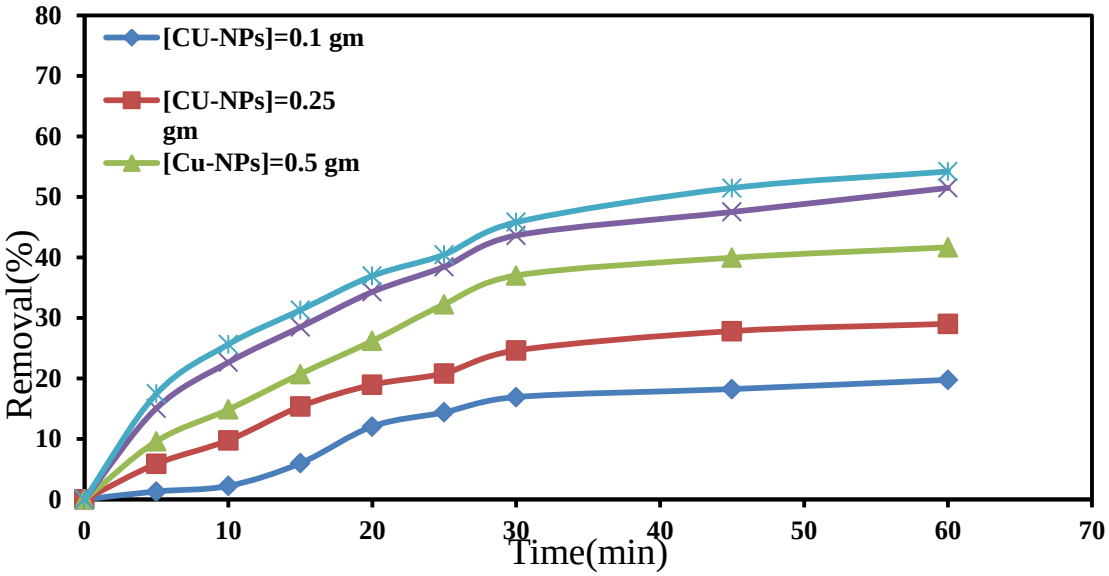

Figure 6: Effects of Cu-NPs dose on the removal % at pH=3, 10 mg/L CIP, 40°C and reaction time 60 min.

3.2.2 Effects of initial solution temperature

The temperature effect on the removal efficiency of the drug was examined at temperatures of 20–50 °C. Figure-7 indicates that the removal efficiency of CIP was altered in response to various temperatures. The CIP removal percentage was increased with increasing temperature by 43%, 43.5%, 78.4%, and 49.3%, at 20, 30, 40, and 50 ° C, respectively. This is because the viscosity of the solution may be lowered by increasing the temperature, which increases mobility by increasing the rate of diffusion of adsorbate through the external limit layer of the adsorbent [34], leading to the increase in adsorption capacity.. The optimal value of temperature was 40° C. A similar observation was noted by an earlier work [35].

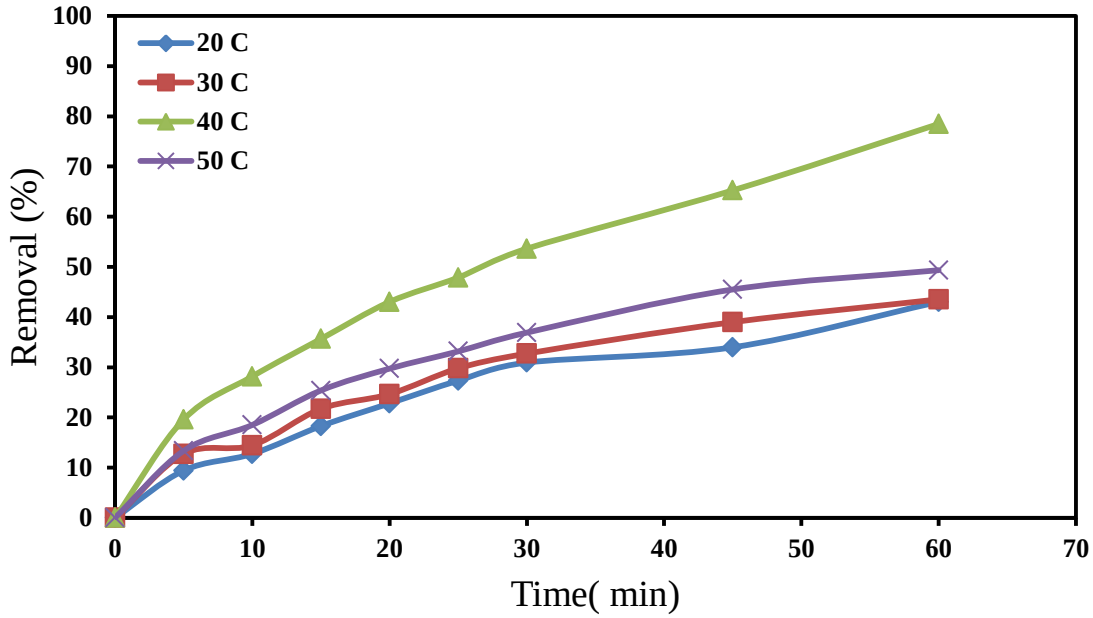

Figure 7: Effects of temperature on the removal % . Experimental conditions: 10 mg/L of CIP, 0.75 gm/L Cu-NPs, pH= 4, and reaction time 60 min.

3.2.2 Effects of initial pH of the solution

The effects of pH of the medium on CIP adsorption using NPs are shown in Figure-8. The results indicate that higher CIP adsorption could be based on two factors:(1) At pH 3, the H^+ concentration in the solution was very high, with an increased electrostatic attraction between the H+ solution and the adsorbent. CIP is achieved by increasing pH solution, so the competition for adsorption sites between H+ and the adsorbate is increased; and (2) At higher pH (>10), OH^- ion concentration is increased and the adsorption is decreased, probably due to the competition between CIP molecules and OH^- ions for the adsorption site [36]. Therefore, a physisorption reaction may occur between the CIP molecules and Cu-NPs active sites at pH=4. The removal efficiency values after sixty minutes at various pH levels (2.5, 3, 4, 5, 7, 8, 9, and 10) are 37%, 51.4%, 78.4%, 50%, 73.6%, 32.6%, 31%, and 27.5%, respectively. A similar observation was noticed in earlier investigations [37, 38].

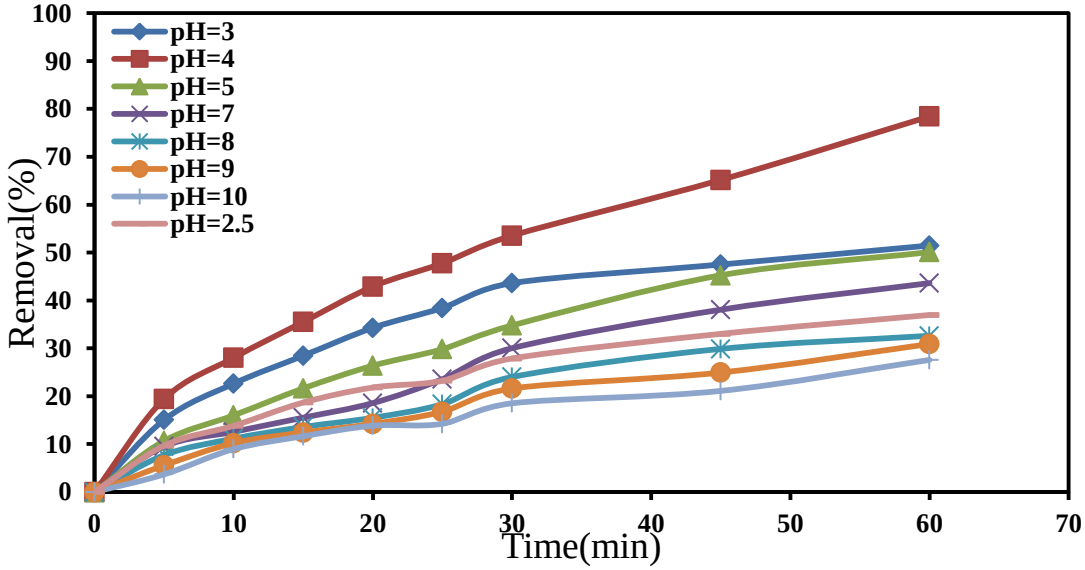

Figure 8-Effects of PH at 0.75 gm Cu-NPs, 10 mg/L of CIP, 40 °C, and 60 min

3.2.3 Effects of CIP initial concentration

Figure-9 illustrates the impact of CIP concentration on removal effectiveness. The CIP removal effectiveness values after 60 minutes of the reaction time were 100, 83, 78.4, and 42.6% at CIP

concentrations of 2, 5, 10, and 15 mg/L. While, after 30 minutes, the removal efficiency was decreased from 72.3, 65.2, 53.5, to 35.8% with the increase in the initial concentration of CIP from 2, 5, 10 to 15 mg/L, respectively. However, increasing the initial concentration to higher than 10 mg/L resulted in a decrease in the removal efficiency, The results obtained are consistent with those described in the literature [38, 39]. The possible cause of these results is the initial CIP concentration and the number of active Cu-NPs sites, as they are likely to increase and lead to competitive adsorption of CIP molecules [33].

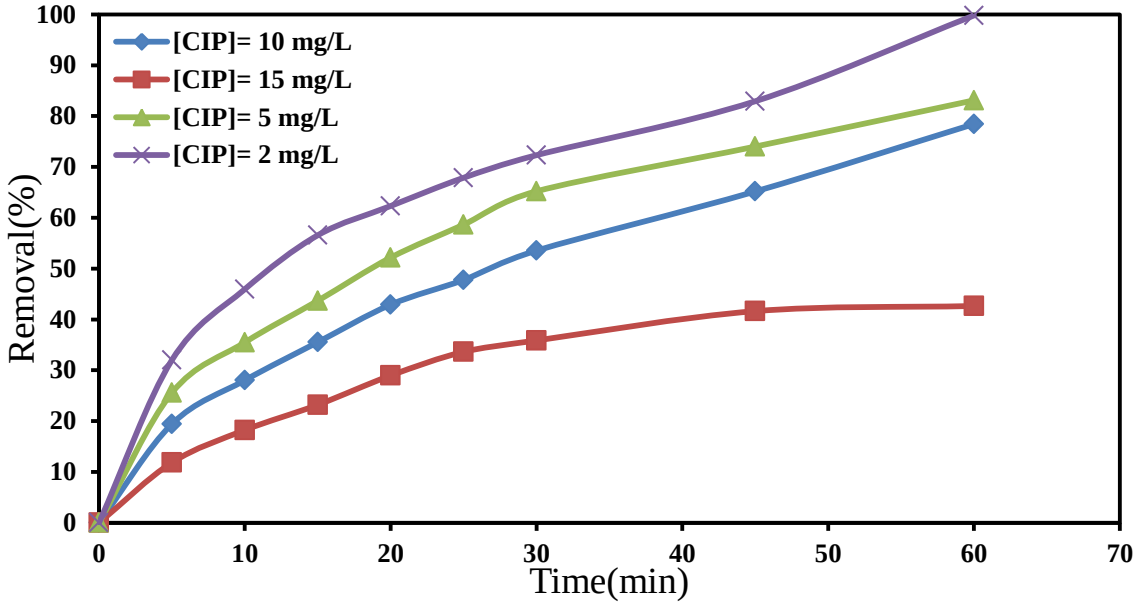

Figure 9: Effects of the initial CIP concentration. Experimental conditions: Temperature 40°C, pH 4, Cu-NPs (0.75 gm/L), and reaction time 60 min.

3.2.4 Effects of contact time

To determine the equilibrium point, the effects of the contact time are extremely important in the adsorption process. Figure-10 shows how the contact time increases at different pH values (4, 7, and 10). The CIP removal efficiency in the batch system increases with additional contact time. The adsorption process was initially rapid due to the driving force of the highest CIP concentration, after which the removal rate slowed for all pH values. This effect is due to the continuous decrease in the number of adsorbent active sites and the concentration of non-adsorbed CIP molecules. After 60 minutes, the CIP removal efficiency at pH values of 4, 7 and 10 were 80.7, 43.6 and 27.5%, while after 180 minutes the values were 92.3, 70.6, and 51%, respectively. A similar observation was found by other authors [27, 35]. The optimal pH value was 4; with a maximum removal efficiency of 80.7% after 60 min and 92.3% after 180 min. Table- 3 lists the results of the removal efficiency of CIP by different adsorbents from previous studies and compares them to the result obtained by the present work.

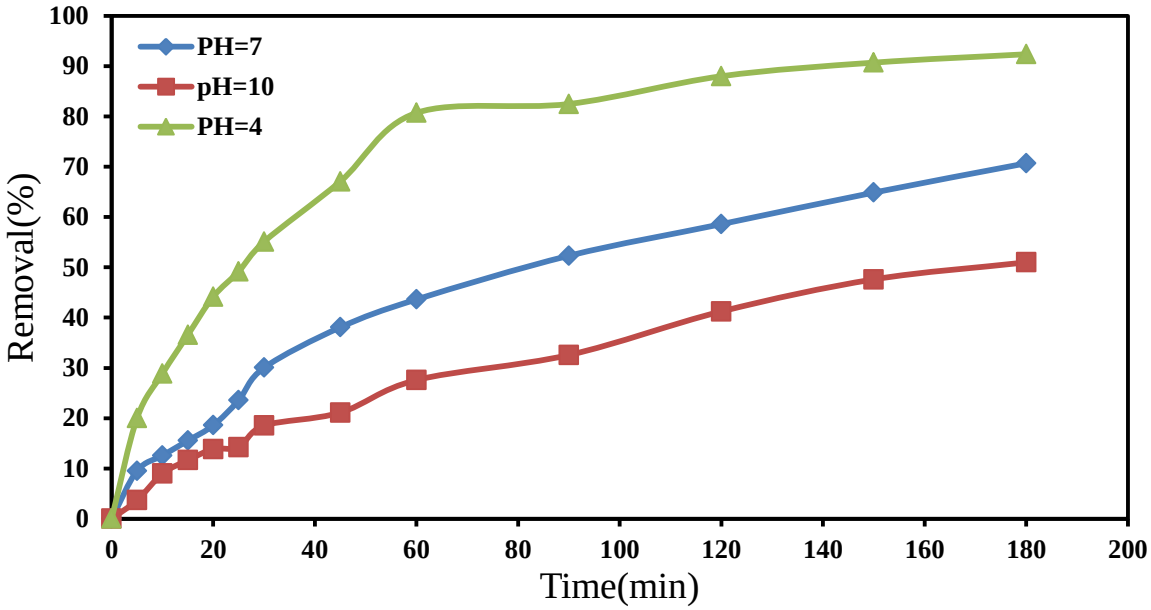

Figure 10-Effects of time at various pH, Experimental conditions: 10 mg/L of CIP, 0.75 gm/L of Cu-NPs, and temperature 40 °C.

Table 3-Summary of the results of the removal efficiency of CIP by different adsorbents from previous studies with a comparison to the result obtained by the present work

Ciprofloxacin(CIP)	Adsorbent	Optimum factor	Major results	References
Ciprofloxacin (CIP)	Sawdust (SD) collected from a local saw-mill	CIP concentration =40 mg/L, dosage=50 mg of sorbent SD, T= 33 ^{o}C, contact time= 1 hr, pH= 5.8	Pseudo-second-order kinetics was the best-fitted model. The intra-particle diffusion was involved in the adsorption processes. Efficiency =85%.	[3]
Ciprofloxacin (CIP)	Chemically carbon from date palm leaflet	CIP concentration =200 mg/L, dosage=0.4 g of sorbent, T= 25 ^{o}C, contact time= 48 hr, pH= 6	Ciprofloxacin was fitted to the Langmuir isotherm model, the process was spontaneous and endothermic, activation energy =17kJ/mol	[40]
Ciprofloxacin (CIP)	Magnetite (Fe_3O_4)	CIP concentration= 0.1 mM, pH=6, dosage= 10 g/L, contact time=24 hr	Adsorption processes. Efficiency =80%.	[41]
Ciprofloxacin (CIP)	Fe3O4 nanoparticles and metal–organic framework loaded on iron oxide nanoparticles	CIP concentration= 250mg/L, pH=6, dosage= 0.5 g/L, contact time=5 hr, T= 298 K.	The Elovich and the pseudo-second-order were the best fitted models, ciprofloxacin was fitted to the Langmuir isotherm model, the process was spontaneous and endothermic.	[42]
Ciprofloxacin (CIP)	Magnesium oxide (MgO) nanoparticles from Sigma Co. (US)	CIP concentration= 10mg/L, pH=6, dosage= 1g/L, contact time=60 min	The Pseudo-second-order model was the best-fitted model, ciprofloxacin was fitted to the Langmuir isotherm model, the removal efficiency =85%.	[22]
Ciprofloxacin (CIP)	Humic acid (HA)- and levulinic acid	CIP concentration= 14 mg/L, pH=8, dosage= 15mg/L, contact	Maximum adsorption capacities =44.6 mg/g for HA-coated Fe_3O_4, and = 40	[43]

	(LA)-coated magnetic Fe_3O_4 nanoparticles	time=40, and 60 min, T= 37 ^oC	mg/g for LA-coated Fe_3O_4. Removal efficiency =100%.	
Ciprofloxacin (CIP)	Copper oxide nanoparticles (CuO)	Initial (CIP) concentration=100 mg/L, pH=4, T=298 K, contact time= 135 min, dosage =100 mg/10ml.	The process follows first-order kinetics, Freundlich isotherm model was the best model, intra-particle diffusion was not the rate-determining step, the process was spontaneous and endothermic, the removal efficiency= 81.5%.	[35]
Ciprofloxacin (CIP)	ZnO nanoparticles and groundnut (Arachis Hypogaea) shell powder	CIP concentration= 100 mg/L, pH=4 for ZnO-NPs, pH=6 for groundnut, contact time =150 min, adsorbent dosage =100 mg, T= 298 K.	Pseudo-first-order kinetics was the best-fitted model, The intra-particle diffusion was not the rate-determining step, the Freundlich isotherm model was the preferred model.	[44]
Tetracycline (TEC), amoxicillin (AMO), and ciprofloxacin (CIP)	Pistachio shell powder that was coated with ZnO nanoparticles (CPS)	Antibiotic concentration= 60mg/L, CPS dose= 0.1g/100mL, pH=5, time=120 min, agitation speed= 150rpm	The kinetic data of the three antibiotics modeled by the pseudo-second-order, the nature of the kinetic adsorption is chemical. The CPS maximum adsorption capacity based on the Langmuir model outcomes for the three antibiotics.	[34]
Ciprofloxacin (CIP)	Copper nanoparticles (Cu-NPs) from green tea leaves extract	Initial (CIP) concentration=10 mg/L, pH=4, T=40 ^OC, contact time= 60 min, dosage =0.75 g/L	A pseudo-first-order model is preferred for the kinetic, the equilibrium data were best fitted with Langmuir and Dubinin isotherm model, the process was spontaneous and endothermic sorption, removal efficiency= 78.4% after 60 min, and 92.3% after 180 min	The present work (2020)

3.3 Adsorption Kinetics

The adsorption kinetics models have been studied. Four kinetic models were evaluated. The linear forms of the pseudo-first-order, the pseudo-second-order [45, 11, 46], Elovich [12,22], and Behnajady-Modirshahla-Ghanbary (BMG) models [19] are given in Eqs. (3– 7), respectively:

$$\text{Log}\,(q_e - q_t) = \log q_e - k_1\, t/2.303 \quad \text{Pseudo-first-order} \quad (3)$$

$$t/q_t = 1/k_2\, q_2^{\,2} + t/q_e \quad \text{Pseudo-second-order} \quad (4)$$

$$t/q_t = 1/h + t/q_e \quad (5)$$

$$q_t = 1/\beta\ \ln(\alpha\beta) + 1/\beta\ \ln(t) \quad \text{Elovich model} \quad (6)$$

$$t/[1 - (C_t/C_0)] = m + b\,(t) \quad \text{BMG model} \quad (7)$$

where q_e and q_t are the amounts of CIP adsorbed on the adsorbent (mg/g) at time t and equilibrium condition, k_1 and k_2 are the rate constants of the first order (min^{-1}) and the second-order adsorption (g/mg. min) respectively, α (mg/g/min) and β (g/mg) are adsorption and desorption rate constants, C_0 and C_t are the concentration of drug at time 0 and time t, respectively, m and b are two constant of BMG model.

The rate constant k_1 (min^{-1}) was calculated from the slope and intercept of Log ($q_e - q_t$) versus t shown in Figure- (11–a). The initial adsorption rate (h) was estimated by pseudo-second-order from equation (5). The h (mg/g min^{-1}) values for the fixed concentration of CIP (15, 10, 5, 2 mg /L) were 0.5333,

0.6922, 1.0102, and 1.3056, respectively. The low k_2 values parallel to h indicated rapid sorption at the beginning, followed by slower adsorption. The rate constants for the pseudo-second-order k_2 and q_e were calculated from the intercept and slope of t / q_t to the t graph, as shown in Figure- (11-b). k_1 (rate constant for the pseudo-first-order) was >k_2 for the pseudo-second-order, while the best-suited equation of Cu-NPs kinetic CIP adsorption was the pseudo-first-order [27]. Table-4 demonstrates that the first-order regression coefficient R^2 (0.9706) is better in comparison to the second-order R^2 (0.9113).

The adsorption rate constant α (mg /g /min) and desorption rate constant β (g / mg) were obtained from the slope and intercept of q_t versus ln (t), as shown in Figure- (11- c). The α and β for 15, 10, 5 and 2 mg / L showed higher adsorption rates (0.8537, 1.5507, 1.9151, 2.3666) as compared to desorption rates (0.7018, 0.4690, 0.4580, 0.4052), respectively. Table-4 shows that the highest regression coefficient value of the Elovich model was 0.9619.

For adsorption of the CIP in different conditions, the parameters m (min) and b of the Behnajady-Modirshahla-Ghanbary (BMG) kinetic models were calculated from the slope and intercept of t versus t /[1-(C_t / C_0)],, as shown in Figure- (11-d). When the concentration of CIP increased from 2 to 15 mg / L, the values for m and b increased from 10.193 to 24.876 and from 0.9379 to 1.9693, respectively. This indicates that the time of the adsorption process is increased when the CIP concentration increases, as shown in Table-4. The kinetic data showed that the BMG model regression coefficient value R^2 is 0.9113, as shown in Table-4. Table-4 shows that the best kinetic pseudo-first-order model is due to the higher R^2 (0.9704) value than other kinetic models. Several research papers [4, 18, 44] have already shown this deviation.

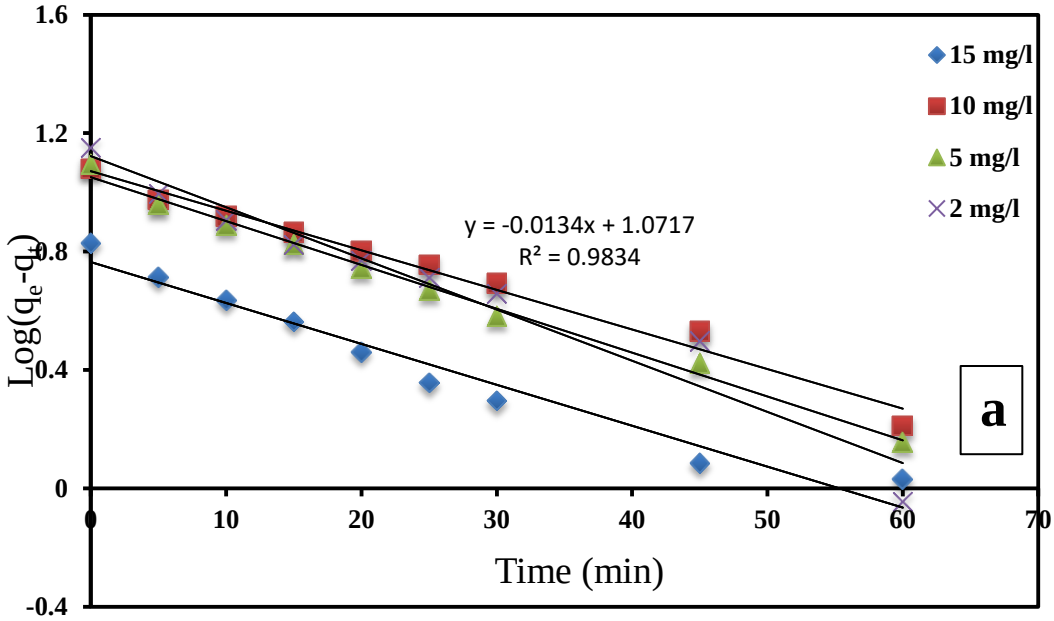

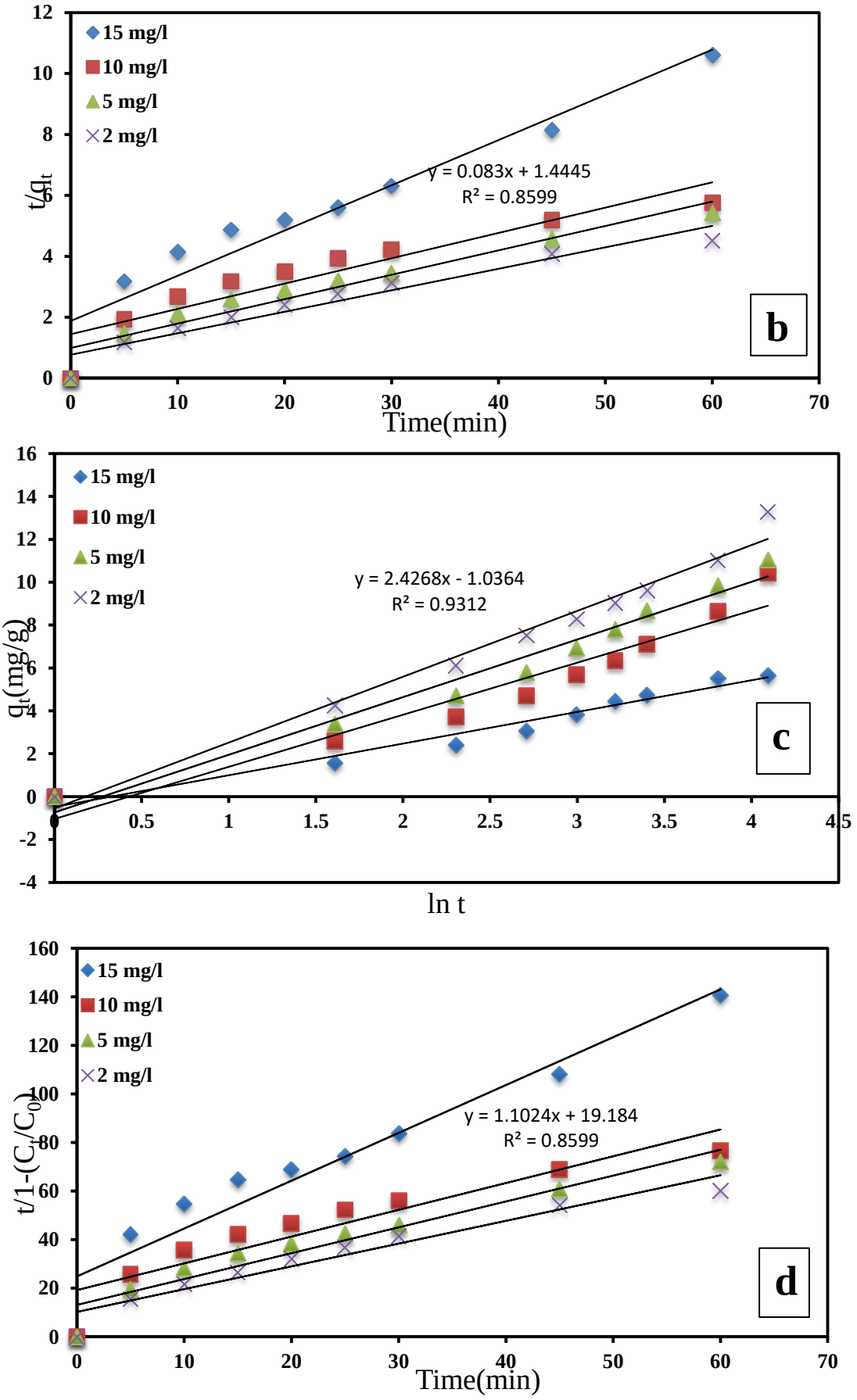

Figure 11- A plot showing **(a)** Pseudo-first-order, **(b)** Pseudo-second-order, **(c)** Elovich, and **(d)** BMG kinetic models for Cu-NPs.

Table 4-The Pseudo-first-order, Pseudo-Second-order, Elovich, and MBG Kinetics parameters for the adsorption of CIP onto Cu-NPs at various initial concentrations of CIP

CIP (mg/L)	R% After 60 min	$q_{e(exp)}$ (mg/g)	Pseudo-first-order			Pseudo-second-order			Elovichs – Model			BMG- Model		
			q_e (mg g^{-1})	k_1 (min^{-1})	R^2	q_e (mg g^{-1})	k_2 (g $mg^{-1}.min^{-1}$)	R^2	α (mg $g^{-1}min^{-1}$)	β (g mg^{-1})	R^2	m (min)	b	R^2
15	42.6 %	5.6586	5.8103	0.03178	0.9584	6.7358	0.0117	0.9251	1.0644	0.6762	0.9642	24.876	1.9693	0.9251
10	78.4 %	10.416	11.7950	0.0308	0.9834	12.0441	0.0047	0.8599	1.5832	0.412	0.9312	19.184	1.1024	0.8599
5	83%	11.048	11.2434	0.0340	0.9926	12.4843	0.0064	0.9269	2.0423	0.3722	0.9722	13.16	1.0648	0.9269
2	100 %	13.280	13.2770	0.0398	0.9475	14.1843	0.0064	0.9335	2.5667	0.3256	0.9801	10.193	0.9379	0.9335
Average R^2					**0.9704**			**0.9113**			**0.9619**			**0.9113**

3.4 Adsorption mechanism

Equations (8) and (9) [47, 35, 18] were used for determining the mechanism of adsorption. Intraparticle diffusion kinetic model:

$$q_t = K_{id}\, t^{0.5} + C \quad (8)$$

Liquid film diffusion kinetic model:

$$\mathrm{Ln}\,(1-q_t/q_e) = -K_{fd}\, t \quad (9)$$

where q_t indicates the amount of CIP molecules adsorbed (mg/ g) at t time (min) and q_e denotes the amount of CIP molecules adsorbed (mg / g) at equilibrium. The intraparticle diffusion constants K_{id} (mg/g $min^{0.5}$) and C (mg /g) indicate the boundary layer thickness, while K_{fd} (m^{-1}) is the fluid film diffusion constant. In the event that the linear trend line is passing or is near to the origin of the trend line (C=0), the intraparticle diffusion is the limiting rate step. The plot of ln ($1-q_t/q_e$) versus t Figure-12-b) obtained slopes and intercepts related to K_{fd} and C [48]. Table-5 shows the results from experimental information with intraparticle and film diffusion at different initial CIP concentrations. It is observed that the straight lines in Figures- (12-a) and (12-b) does not pass through the original line. This observation indicates that the adsorbing process is controlled by the thickness of the limit layer, while the high regression coefficient values suggest that the intraparticle diffusion (R^2=0.9879) is more applicable [27]. The C values indicate that the spread liquid film diffusion may also be involved in the process of adsorption. The diffusion of the intraparticles is not the only rate control process. Other adsorption and diffusion mechanisms have been described in various research papers [27, 49].

Table 5-The adsorption mechanism of intraparticle - model and liquid film diffusion at various initial concentrations of CIP

CIP (mg/L)	Intraparticle diffusion			Liquid Film diffusion		
	K_{id}(mg/g.$min^{0.5}$)	C(mg/g)	R^2	K_{fd} (min^{-1})	C(mg/g)	R^2
15	0.7982	0.0498	0.9727	0.0318	-0.1481	0.9584
10	1.349	0.3249	0.9963	0.0308	-0.0212	0.9834
5	1.4592	0.1978	0.9931	0.0341	-0.1047	0.9926
2	1.6584	0.559	0.9895	0.0398	-0.0662	0.9475
Average R^2			0.9879			0.9704

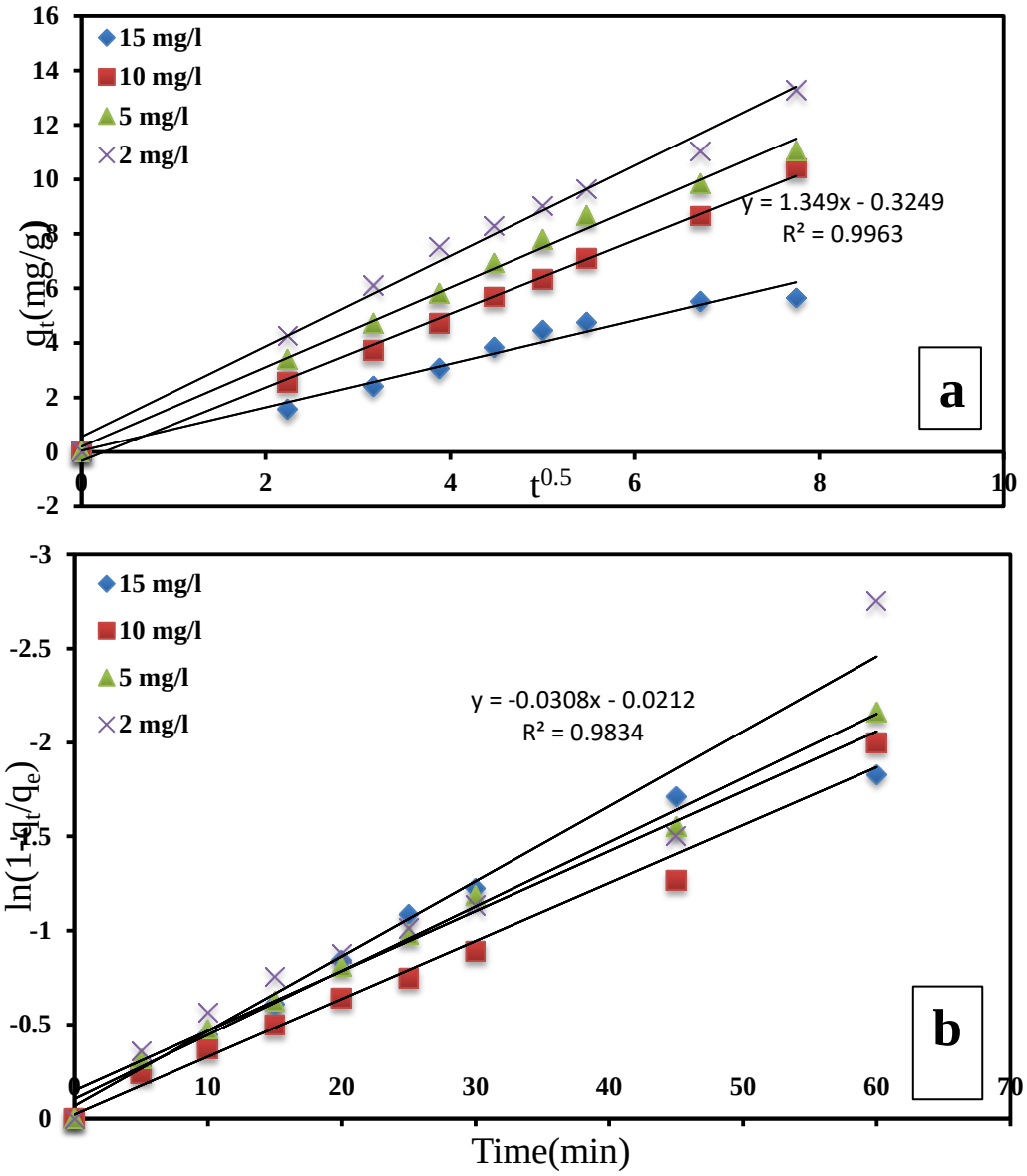

Figure 12- (a) The intraparticle diffusion and **(b)** liquid film diffusion information of CIP adsorption onto Cu-NPs.

3.5 Adsorption Isotherm

Langmuir, Freundlich, and Temkin isotherm models were designed for ciprofloxacin [20, 50] and Dubinín isotherms [46, 51].

Langmuir model calculation is shown by equation 10.

$$C_e/q_e=1/ q_{max} b +C_e/ q_{max} \quad (10)$$

Dimensionless constant or separation factor (R_L) calculation is shown by equation 11.

$$R_L=1/ (1+bC_0) \quad (11)$$

Freundlich model calculation is shown by equation 12.

$$\text{Log } q_e= (1/n) \log C_e+ \log k_F \quad (12)$$

Temkin model calculation is shown by equation 13.

$$q_e= (RT/B_T) \ln C_e + (RT/B_T) \ln K_T \quad (13)$$

Dubinin model calculation is shown by the following equations.

$$\text{Ln } q_e = \ln q_m-\beta\varepsilon^2 \quad (14)$$

$$\varepsilon =RT \ln (1+1/C_e) \quad (15)$$

$$E=1/ \sqrt{(-2\beta)} \quad (16)$$

where C_e and q_e are the concentration and amount adsorbed of CIP at equilibrium. q_{max} and b are Langmuir constants. These values were calculated from the slope and intercept of the graph that plotted C_e/q_e versus C_e, as shown in Figure- (13-a). The results were well defined by Langmuir isotherm, where (R^2) value is higher by using Langmuir as compared to Freundlich. Homogeneous adsorbent surfaces should exist on Langmuir with the same adsorption sites. The Freundlich isotherm is an empirical equation that is supposed to perform the adsorption procedure on the heterogeneous surface through a multilayer adsorption mechanism. As shown in Table-6, Langmuir constant b was established at 2.1307 for Cu-NPs. The adsorption nature of the R_L indications are unfavorable when $R_L > 1$, linear when $R_L = 1$, favourable when $0 < R_L < 1$, or irreversible when $R_L = 0$, where R_L is a dimensionless constant usually referred to as the separation factor [46]. The R_L value achieved for Cu-NPs adsorption was in the range of 0.04504-0.0449; therefore, CIP adsorption was favorable for adsorbents as they ranged between 0 and 1. The maximum uptake (q_{max}) was 5.5279 mg of CIP per gram of the Cu-NPs.

The Freundlich coefficient values k_F and n were determined from the slope and intercept, as shown in Figure- (13-b), as these values have an important effect on adsorption favorability. The constant n is effective for adsorption, where n values of 2-10 are generally good, 1-2 indicate quite difficult adsorption, and less than 1 indicates poor adsorption. Thus, the obtained value of n= -9.4607 indicates poor adsorption.

K_T (L/gm) and B_T (kJ/mol) are values of maximum binding energy coefficients and sorption heat, respectively. These values were calculated from the slope and intercept of the plotted graph of q_e versus ln C_e in Figure- (13-c). K_T and B_T values are defined in (Table- 6), with minute changes in sorption heat and robust interactions between adsorbate and adsorbent.

q_m and β can be determined from the intercept and slope of the plotted graph ln q_e vs. ε^2 shown in Figure- (13-d). From Eq.15, the E value was 0.8409kJ / mol, which indicates physical adsorption. Figure- (13a-d) shows four models of adsorption isotherms, together with experimental CIP data. The Dubinin and Langmuir models provided the better fitting in terms of R^2 (0.9963 and 0.9626, respectively) with maximum adsorption capacity q_{max} = 1.1069 and 5.5279 mg/g, respectively. A similar observation was noticed in various researches [52-54].

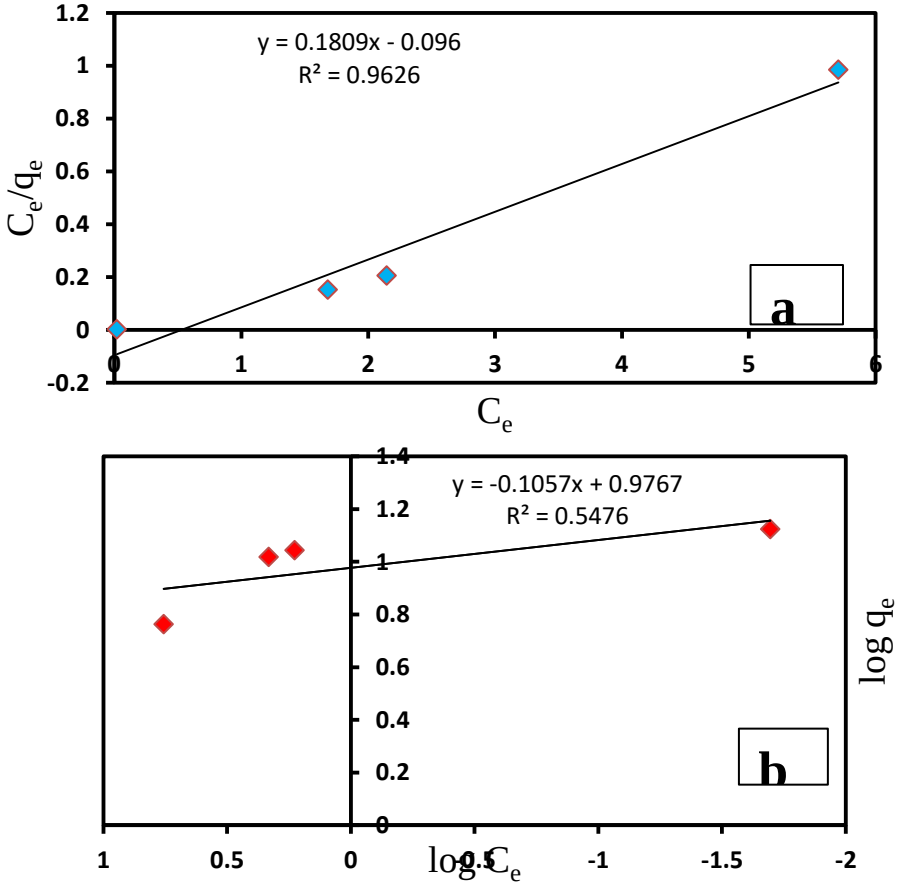

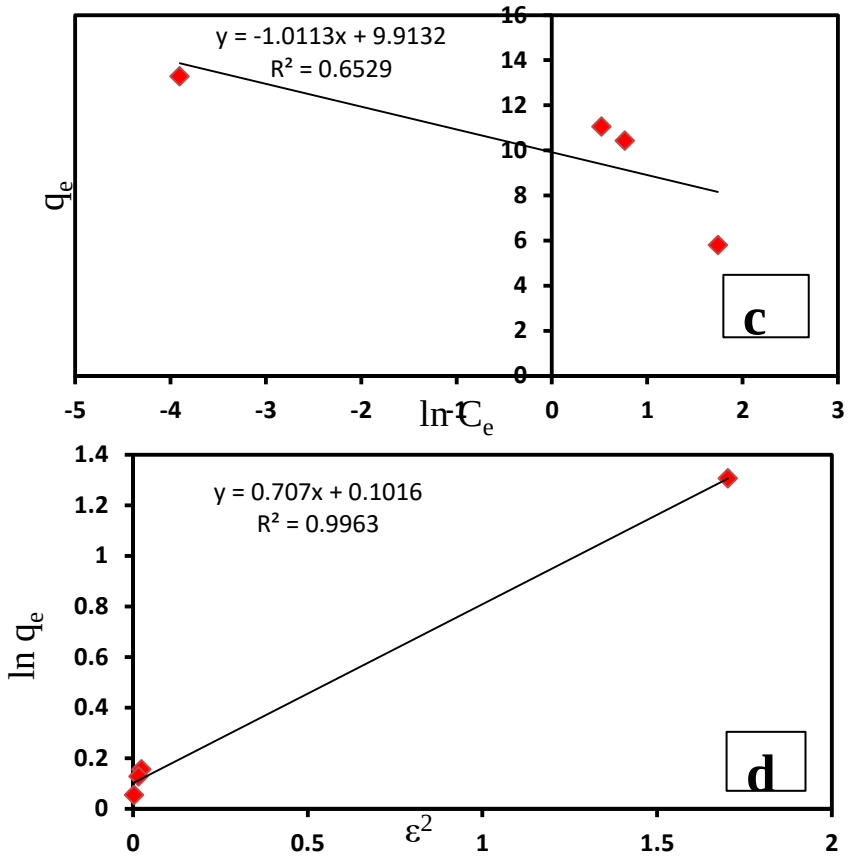

Figure 13-A plot showing **(a)** Langmuir, **(b)** Freundlich, **(c)** Temkin and, **(d)** Dubinin isotherm models for Cu-NPs.

Table 6- Isotherm parameters values for different model

Langmuir			**Freundlich**		
q_{max} (mg g^{-1})	**B (L mg^{-1})**	**R^2**	**k_F**	**n**	**R^2**
5.5279	2.1307	0.9626	9.4776	-9.4607	0.5476
Temkin			**Dubinin**		
K_T(L/g)	**B_T (kJ/mol)**	**R^2**	**q_m (µg/g)**	**E (kJ/mol)**	**R^2**
5.53169E-05	-0.3288	0.6529	1.1069	0.8409	0.9963

3.6.Adsorption Thermodynamics

The adsorption behaviors of different concentrations of CIP onto Cu-NPs were explored at 298, 303, 313 and 323 K. The thermodynamic parameters of enthalpy, entropy, and Gibbs free energy were calculated from equations 17 to 19 [55, 20, 56].

$$\Delta G^0 = -RT \ln K_{eq} \quad (17)$$

$$K_{eq} = q_e/C_e \quad (18)$$

$$\text{Ln } K_{eq} = -\Delta H^0/RT + \Delta S^0/R \quad (19)$$

where T, R, and K_{eq} are absolute temperature (K), universal gas constants (0.008314 kJ / mol K^{-1}), and the distribution coefficient, respectively. C_e and q_e (mg /g) are the equilibrium concentration and the amount of adsorbent at equilibrium, respectively. Gibbs free energy (ΔG^0) was calculated using ln

K_{eq} values for different temperatures. Enthalpy (ΔH^0) and entropy (ΔS^0) were determined from the slope and intercept connected to ΔH^0 and ΔS^0 of the plot of ln K_{eq} versus 1/T, as shown in Figure- (14-a), according to Eq.19. Table-7 shows the values of free energy, enthalpy, and entropy. The positive ΔH^0 value showed favorable and endothermic sorption. The negative free energy (ΔG^0) indicates the spontaneous nature of the CIP adsorption on Cu-NPs [53, 55, and 56]. The positive entropy (ΔS^0) change indicates the increase in interruption at the solid-liquid interface during the adsorption process [52]. The activation energy (E_a) was calculated by applying Eq.21 [57, 58, and 39]. A is the Arrhenius factor, R is the gas constant (8,314 J/mol. K), K is the temperature in Kelvin, Ea is the activation energy (kJ/mol), and k_{obs} (min^{-1}) is the rate constant calculated from Eq. 20. E_a is calculated by the slope and intercept of ln(C_t / C_0) against time t(min). The straight line of ln k_{obs} against 1/T, shown in Figure-(14-b), the activation energy is 13.22 kJ/mol, indicating controlled diffusion process, whereas a value of E_a greater than 20 kJ / mol is attributed to a processes with chemical controls [59, 53].

$$\ln (C_t / C_0) = -k_{obs}\, t \quad (20)$$

$$\ln k_{obs} = \ln A - E_a/RT \quad (21)$$

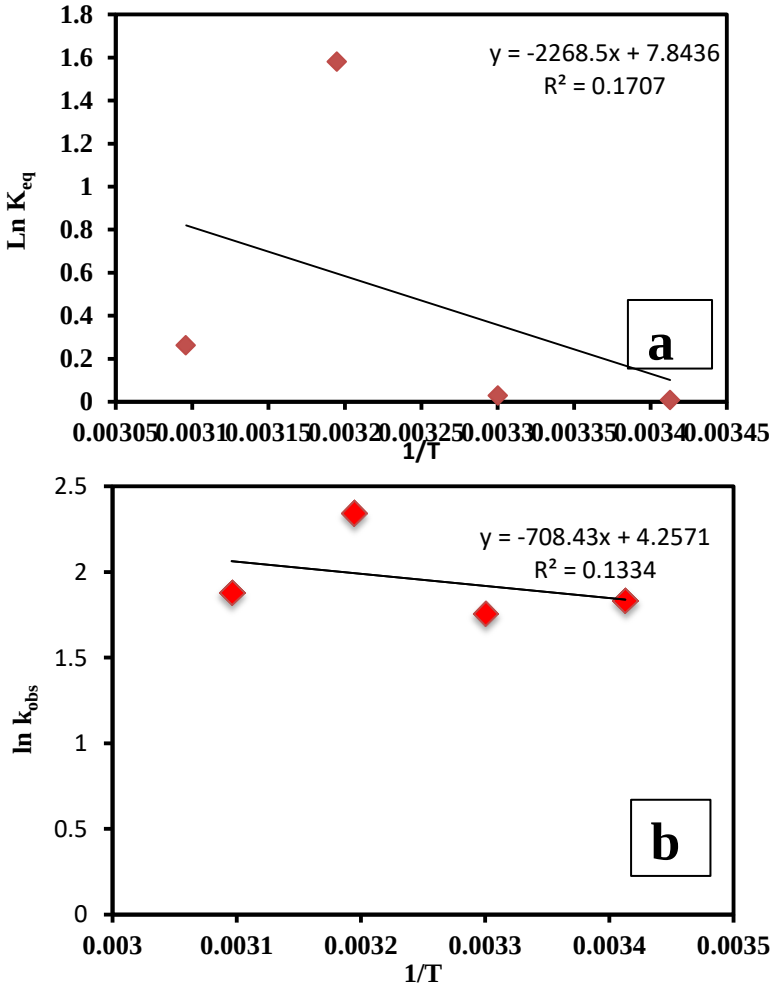

Figure 14- Relationship between **(a)** Ln K_{eq} against 1/T for thermodynamic constants determination of CIP adsorption onto Cu-NPs, **(b)** ln k_{obs} against 1/T to estimate E_a at the initial concentration of 10 mg/L, pH=4, and 300 rpm for adsorption of CIP with a dose of 0.75 gm and 60 min contact time.

Table 7- Thermodynamic examination of the adsorption of CIP onto Cu-NPs(initial concentration 10 mg/L, Cu-NPs dose 0.75g/L, contact time 60 min, agitation speed 300 rpm, and pH=4).

ΔG^0(kJ/mol)				ΔH^0(kJ/mol)	ΔS^0(kJ/mol.K)
T=20°C	T=30°C	T=40°C	T=50°C	18.8603	0.0652
-0.0166	-0.0691	-4.1084	-0.7014		

Conclusions

This study examined the adsorbent performance of Cu-NPs in the batch system concerning CIP adsorption. Advanced SEM, AFM, BET, zeta potentials, and FT-IR analyses were used to characterize the Cu-NPs adsorbent. The characterization results show that the Cu-NPs nanoparticles have positive effects in terms of use and adsorption on the prepared adsorbents. The parameters of the adsorption process were optimized with pH, contact time, initial antibiotic concentration, temperature, and Cu-NPs dose values of 4, 60 min, 10 mg/L, 40°C, and 0.75 gm/L, respectively). The isothermal, kinetic, and thermodynamic studies were conducted based on the data of the optimized impact study. The isothermal study show that the surface of Cu-NPs consists of a homogenous adsorption site that is ready for reaction of antibiotic molecules. The mechanism of the adsorption process was the intraparticle diffusion process. The spontaneous and endothermal nature of the adsorption process was underlined by the thermodynamic element. In future studies, one should identify the effects of the agitation speed, the size of nanoproducts, and the size of the magnetic bar on the adsorption of Cu-NPs as a result of the kinetic data were modeled and the adsorption trend was observed to obey the Pseudo-first order kinetic model for CU-NPs indicating the physisorption mechanism onto this adsorbent for the drug (CIP) studied.

References

1. Frade, V. M. F. *et al.* **2014**. 'Environmental contamination by fluoroquinolones', *Brazilian Journal of Pharmaceutical Sciences*, **50**(1): 41–54. doi: 10.1590/s1984-82502011000100004.
2. Shalini, K. *et al.* **2010**. 'A review on pharma pollution', *International Journal of PharmTech Research*, **2**(4): 2265–2270.
3. Bajpai, S. K., Bajpai, M., and Rai, N. **2012**. 'Sorptive removal of ciprofloxacin hydrochloride from simulated wastewater using sawdust: Kinetic study and effect of pH', *Water SA*, **38**(5): 673–682. DOI: 10.4314/wsa.v38i5.4.
4. Dessouki, H. A. *et al.* **2014**. 'Photocatalytic Degradation of Metronidazole in Aqueous Solutions by Copper oxide nanoparticles', *Journal of Basic and Environmental Sciences*, **1**(January): 102–110. Available at: http://jbesci.org/published/1.4.1.pdf.
5. El-Kemary, M., El-Shamy, H. and El-Mehasseb, I. **2010**. 'Photocatalytic degradation of ciprofloxacin drug in water using ZnO nanoparticles', *Journal of Luminescence*. Elsevier, **130**(12): 2327–2331. DOI: 10.1016/j.jlumin.2010.07.013.
6. Sun, Y. *et al.* **2014**. 'Adsorption and coadsorption of ciprofloxacin and Ni(II) on activated carbon-mechanism study', *Journal of the Taiwan Institute of Chemical Engineers*. Taiwan Institute of Chemical Engineers, **45**(2): 681–688. DOI: 10.1016/j.jtice.2013.05.013.
7. Van Wieren, E. M., Seymour, M. D. and Peterson, J. W. **2012**. 'Interaction of the fluoroquinolone antibiotic, ofloxacin, with titanium oxide nanoparticles in water: Adsorption and breakdown', *Science of the Total Environment*. Elsevier B.V., **441**: 1– DOI: 10.1016/j.scitotenv.2012.09.067.
8. Ahalya, Chemistry, O. F. and Ramachandra, T. V. **2003**. 'Biosorption of Heavy Metals Biosorption of Heavy Metals', *Research Journal Of Chemistry And Environment*, **7**(4): 71–79.
9. Zou, C. *et al.* **2019**. 'Removal of Pb(II) from aqueous solutions by adsorption on magnetic bentonite', *Environmental Science and Pollution Research*, **26**(2): 1315–1322. DOI: 10.1007/s11356-018-3652-0.
10. Ghorai, S., Sarkar, A. K. and Pal, S. **2014**. 'Rapid adsorptive removal of toxic Pb2+ ion from aqueous solution using recyclable, biodegradable nanocomposite derived from templated partially hydrolyzed xanthan gum and nano silica', *Bioresource Technology*. Elsevier Ltd, **170**: 578–582. DOI: 10.1016/j.biortech.2014.08.010.
11. De Gisi, S. *et al.* **2016**. 'Characteristics and adsorption capacities of low-cost sorbents for wastewater treatment: A review', *Sustainable Materials and Technologies*. Elsevier B.V., **9**: 10–40. DOI: 10.1016/j.susmat.2016.06.002.
12. Salata, O. V. **2004**. *Journal of Nanobiotechnology*, **6**(3): 1–6. DOI: 10.1186/1477-3155-2-12.
13. Christian, P. *et al.* **2008**. 'Nanoparticles: Structure, properties, preparation, and behavior in environmental media', *Ecotoxicology*, **17**(5): 326–343. DOI: 10.1007/s10646-008-0213-1.
14. Loo, Y. Y. *et al.* **2012**. 'Synthesis of silver nanoparticles by using tea leaf extract from Camellia Sinensis', *International Journal of Nanomedicine*, **7**: 4263–4267. DOI: 10.2147/IJN.S33344.
15. Khani, R. *et al.* **2018**. 'Green synthesis of copper nanoparticles by fruit extract of Ziziphus spina-

christi (L.) Willd.: Application for adsorption of triphenylmethane dye and antibacterial assay', *Journal of Molecular Liquids*, **255**: 541–549. doi: https://doi.org/10.1016 /j.molliq. 2018.02.010.

16. Suárez-Cerda, J. *et al.* **2017**. 'A green synthesis of copper nanoparticles using native cyclodextrins as stabilizing agents', *Journal of Saudi Chemical Society*. King Saud University, **21**(3): 341–348. DOI: 10.1016/j.jscs.2016.10.005.

17. Rose, A. L., Priya, F. J. and Vidhya, S. **2017**. 'Comparative Study on the Synergistic Action of Differentially Synthesized Copper Nanoparticles With Escherichia Coli and Staphylococcus Aureus', *International Research Journal of Pharmacy*, **8**(11): 85–90. DOI: 10.7897/2230-8407.0811223.

18. Ali, I., Al-Othman, Z. A. and Alwarthan, A. **2016**. 'Synthesis of composite iron nano adsorbent and removal of ibuprofen drug residue from water', *Journal of Molecular Liquids*. Elsevier B.V., **219**: 858–864. DOI: 10.1016/j.molliq.2016.04.031.

19. Hassan, A. K. *et al.* **2019**. 'Kinetic of the degradation of sulfanilic acid azochromotrop (SPADNS) by Fenton process coupled with ultrasonic irradiation or L-cysteine acceleration', *Environmental Technology and Innovation*. Elsevier B.V., **15**: 100380. DOI: 10.1016/j.eti.2019.100380.

20. Wang, H. *et al.* **2014**. 'Surface properties and dissolution kinetics of tea polyphenols', *Journal of Adhesion Science and Technology*, **28**(24): 2416–2423. doi: 10.1080/01694243.2014.968420.

21. Qassim, A. W. (2015) 'Spectrophotometric Determination of Ciprofloxacin Hydrochloride InPharmaceutical Formulation Ciproxin', *International Journal of Advanced Scientific and Technical Research*, **3**(5): 135–146.

22. Khoshnamvand, N., Ahmadi, S. and Mostafapour, F. K. **2017**. 'Kinetic and isotherm studies on ciprofloxacin an adsorption using magnesium oxide nanoparticles', *Journal of Applied Pharmaceutical Science*, **7**(11): 79–83. DOI: 10.7324/JAPS.2017.71112.

23. Asghar, Muhammad Asif *et al.* **2018**. 'Iron, copper and silver nanoparticles: Green synthesis using green and black tea leaves extracts and evaluation of antibacterial, antifungal, and aflatoxin B1 adsorption activity', *LWT - Food Science and Technology*. Elsevier, **90**(January): 98–107. DOI: 10.1016/j.lwt.2017.12.009.

24. Aksu Demirezen, D., Yıldız, Y. Ş. and Demirezen Yılmaz, D. **2019**. 'Amoxicillin degradation using green synthesized iron oxide nanoparticles: Kinetics and mechanism analysis', *Environmental Nanotechnology, Monitoring and Management*, **11**(September 2018). DOI: 10.1016/j.enmm.2019.100219.

25. Kalpana, V. N. *et al.* **2016**. 'Synthesis and characterization of copper nanoparticles using Tridax procumbens and its application in degradation of bismarck brown', *International Journal of ChemTech Research*, **9**(9): 498–507.

26. Sinha, T. and Ahmaruzzaman, M. **2015**. 'Green synthesis of copper nanoparticles for the efficient removal (degradation) of dye from aqueous phase', *Environmental Science and Pollution Research*, **22**(24): 20092–20100. DOI: 10.1007/s11356-015-5223-y.

27. Hossain, M. A. *et al.* **2012**. 'Adsorption and desorption of copper(II) ions onto garden grass', *Bioresource Technology*. Elsevier Ltd, **121**: 386–395. DOI: 10.1016/j.biortech.2012.06.119.

28. Aljeboree, A. M., Alshirifi, A. N. and Alkaim, A. F. **2017**. 'Kinetics and equilibrium study for the adsorption of textile dyes on coconut shell activated carbon', *Arabian Journal of Chemistry*. King Saud University, **10**: S3381–S3393. DOI: 10.1016/j.arabjc.2014.01.020.

29. KSV, G. **2017**. 'Green Synthesis of Iron Nanoparticles Using Green Tea leaves Extract', *Journal of Nanomedicine & Biotherapeutic Discovery*, **07**(01): 1–4. DOI: 10.4172/2155-983x.1000151.

30. PLATON, N. *et al.* **2017**. 'Chemically Modified Clays Used for Environmental Quality', *Journal of Engineering Studies and Research*, **19**(4): 2013. DOI: 10.29081/jesr.v19i4.103.

31. Shih, Y. H., Hsu, C. Y. and Su, Y. F. **2011**. 'Reduction of hexachlorobenzene by nanoscale zero-valent iron: Kinetics, pH effect, and degradation mechanism', *Separation and Purification Technology*. Elsevier B.V., **76**(3): 268–274. DOI: 10.1016/j.seppur.2010.10.015.

32. Abdel-Aziz, H. M., Farag, R. S., and Abdel-Gawad, S. A. **2019**. 'Carbamazepine Removal from Aqueous Solution by Green Synthesis Zero-Valent Iron/Cu Nanoparticles with Ficus Benjamina Leaves' Extract', *International Journal of Environmental Research*. Springer International Publishing, **13**(5): 843–852. DOI: 10.1007/s41742-019-00220-w.

33. Weng, X. *et al.* **2013**. 'Synthesis of iron-based nanoparticles by green tea extract and their degradation of malachite', *Industrial Crops, and Products*. Elsevier B.V., **51**: 342–347. DOI:

10.1016/j.indcrop.2013.09.024.

34. Mohammed, A. A. and Kareem, S. L. **2019**. 'Adsorption of tetracycline fom wastewater by using Pistachio shell coated with ZnO nanoparticles : Equilibrium , kinetic and isotherm studies', *Alexandria Engineering Journal*. Faculty of Engineering, Alexandria University, **58**(3): 917–928. DOI: 10.1016/j.aej.2019.08.006.

35. Sharma, N. and Dhiman, N. **2017**. 'Kinetic and Thermodynamic Studies for Ciprofloxacin Hydrochloride Adsorption from Aqueous Solution on CuO Nanoparticles', **10**(5): 98–106.

36. Ye, S., Lv, X. and Zhou, A. **2009**. 'In Vitro Evaluation of the Efficacy of Sodium Humate as an Aflatoxin B1 Adsorbent', *Australian Journal of Basic and Applied Sciences*, **3**(2): 1296–1300.

37. Batool, M. **2018**. 'Degradation of Malachite Green by Green Synthesized Copper Nanoparticles by Using Aloe Barbadensis Leaf Extracts', *Archives of Nanomedicine: Open Access Journal*, **1**(2): 29–34. DOI: 10.32474/anoaj.2018.01.000108.

38. Batool, M. *et al.* **2019**. 'Adsorption of Congo red (acid red 28) azodye on biosynthesized copper oxide nanoparticles', *Asian Journal of Chemistry*, **31**(3): 707–713. DOI: 10.14233/ ajchem. 2019.21752.

39. Mandava, K. *et al.* **2017**. 'Green Synthesis of Stable Copper Nanoparticles and Synergistic Activity with Antibiotics', *Indian Journal of Pharmaceutical Sciences*, **79**(5): 695–700. doi: 10.4172/pharmaceutical-sciences.1000281.

40. El-Shafey, E. S. I., Al-Lawati, H. and Al-Sumri, A. S. **2012**. 'Ciprofloxacin adsorption from aqueous solution onto chemically prepared carbon from date palm leaflets', *Journal of Environmental Sciences (China)*. The Research Centre for Eco-Environmental Sciences, Chinese Academy of Sciences, **24**(9): 1579–1586. doi: 10.1016/S1001-0742(11)60949-2.

41. Rakshit, S. *et al.* **2013**. 'Mechanisms of ciprofloxacin removal by nano-sized magnetite', *Journal of Hazardous Materials*. Elsevier B.V., 246–247, pp. 221–226. doi: 10.1016/j.jhazmat.2012. 12.032.

42. Moradi, S. E. *et al.* **2016**. 'Effective removal of ciprofloxacin from aqueous solutions using magnetic metal–organic framework sorbents: mechanisms, isotherms and kinetics', *Journal of the Iranian Chemical Society*. Springer Berlin Heidelberg, **13**(9): 1617–1627. doi: 10.1007/s13738-016-0878-y.

43. Danalıoğlu, S. T. *et al.* **2017**. *Removal of ciprofloxacin from aqueous solution using humic acid- and levulinic acid- coated Fe3O4 nanoparticles*, *Chemical Engineering Research and Design*. doi: 10.1016/j.cherd.2017.05.018.

44. Dhiman, N. and Sharma, N. **2018**. 'Batch adsorption studies on the removal of ciprofloxacin hydrochloride from aqueous solution using ZnO nanoparticles and groundnut (Arachis hypogaea) shell powder: a comparison*', *Indian Chemical Engineer*. Taylor & Francis, **61**(1): 67–76. DOI: 10.1080/00194506.2018.1424044.

45. Cheng, M. *et al.* **2019**. 'Highly efficient removal of ceftiofur sodium using a superior hydroxyl group functionalized ionic liquid-modified polymer', *Science of the Total Environment*. Elsevier B.V., **662**: 324–331. DOI: 10.1016/j.scitotenv.2019.01.223.

46. Kowanga, K. D. *et al.* **2016**. 'Kinetic, sorption isotherms, pseudo-first-order model and pseudo-second-order model studies of Cu (II) and Pb (II) using defatted Moringa oleifera seed powder', *The Journal of phytopharmacology*, **5**(2): 71–78. Available at: www.phytopharmajournal.com.

47. Leili, M., Fazlzadeh, M. and Bhatnagar, A. **2018**. 'Green synthesis of nano-zero-valent iron from Nettle and Thyme leaf extracts and their application for the removal of cephalexin antibiotic from aqueous solutions', *Environmental Technology (United Kingdom)*, **39**(9): 1158–1172. DOI: 10.1080/09593330.2017.1323956.

48. Liu, C. **2014**. 'Metal Ions Removal from Polluted Waters by Sorption onto Exhausted Coffee Waste. Application to Metal Finishing Industries Wastewater Treatment'. DOI: http://dx.doi.org/10.1176/appi.ps.201200235.

49. Yaacoubi, H. *et al.* **2015**. 'Adsorption isotherm, kinetic and mechanism studies of 2-nitrophenol on sedimentary phosphate', *Mediterranean Journal of Chemistry*, **4**(6): 289–296. DOI: 10.13171/ mjc.4.6/0151123/sebti.

50. Raju, C., Nooruddin, S. and Babu, K. S. **2017**. 'Studies on leaf extract mediated synthesis of copper nanoparticles for the removal of Bromo cresol green dye from synthetic wastewaters', *Ijsetr*, **6**(10): 1404–1411.

51. Khodadadi, M. *et al.* **2019**. 'A comparative study of using barberry stem powder and ash as adsorbents for adsorption of humic acid', *Environmental Science and Pollution Research*. Environmental Science and Pollution Research, **26**(25): 26159–26169. DOI: 10.1007/s11356-019-05879-4.

52. Homem, V., Alves, A. and Santos, L. **2010**. 'Amoxicillin removal from aqueous matrices by sorption with almond shell ashes1', *International Journal of Environmental Analytical Chemistry*, **90**(14): 1063–1084. doi: 10.1080/03067310903410964.

53. Hao, Y. M., Man, C. and Hu, Z. B. **2010**. 'Effective removal of Cu (II) ions from aqueous solution by amino-functionalized magnetic nanoparticles', *Journal of Hazardous Materials*. Elsevier B.V., **184**(1–3): 392–399. doi: 10.1016/j.jhazmat.2010.08.048.

54. Kamar, F. H. *et al.* **2017**. 'Aqueous Phase Biosorption of Pb(II), Cu(II), and Cd(II) onto Cabbage Leaves Powder', *International Journal of Chemical Reactor Engineering*, **15**(2): DOI: 10.1515/ijcre-2015-0178.

55. Ghadim, E. E. *et al.* **2013**. 'Adsorption properties of tetracycline onto graphene oxide: Equilibrium, kinetic and thermodynamic studies', *PLoS ONE*, **8**(11): 1–9. DOI: 10.1371 /journal .pone.0079254.

56. Murcia-Salvador, A. *et al.* **2019**. 'Adsorption of Direct Blue 78 using chitosan and cyclodextrins as adsorbents', *Polymers*, **11**(6). DOI: 10.3390/polym11061003.

57. Wang, J. *et al.* **2018**. 'Arsenic removal from water/wastewater using layered double hydroxide derived adsorbents, a critical review', *RSC Advances*. Royal Society of Chemistry, **8**(40): 22694–22709. DOI: 10.1039/c8ra03647k.

58. Wang, J. *et al.* **2014**. 'Synthesis and characterization of an inorganic/organic-modified bentonite and its application in methyl orange water treatment', *Desalination and Water Treatment*, **52**(40–42): 7660–7672. DOI: 10.1080/19443994.2013.830690.

59. Liu, X. *et al.* **2013**. 'Remediation of Direct Black G in wastewater using kaolin-supported bimetallic Fe/Ni nanoparticles', *Chemical Engineering Journal*, **223**: 764–771. DOI: https://doi.org/10.1016/j.cej.2013.03.002.